Superradiance from a cylindrically shaped cloud of N two-level atoms

Jamal T. Manassah*
Department of Electrical Engineering, City College of New York, New York 10031, USA
(Received 26 July 2010; published 15 November 2010)

Using the eigenmodes of the scalar-photon kernel of interacting N two-level atoms in a cylindrical configuration, I obtain the time dependence of the superradiant emission for this geometry in two cases of interest. In particular, I consider first the case when one or two eigenmodes dominate the system's dynamics for an inverted system which has been initially prepared in an isotropic state and show that for certain values of the radius of the cylinder ($r = m\lambda, m$ integer) one obtains temporal modulation in the state function. In the second case of interest, I show that the angular distribution of the state function of a system initially prepared in a phased state appears to be chaotic; however, I show that this behavior is due to the high multiplicity of modes having close values for their amplification coefficients.

DOI: 10.1103/PhysRevA.82.053816 PACS number(s): 42.50.Ct, 42.50.Nn

I. INTRODUCTION

The theoretical analysis based on the eigenmodes of the kernel describing the interaction between a two-level atom in the excited state and the same atom in the ground state proved a powerful tool for analyzing the collective dynamics of N two-level atoms. This technique facilitated, inter alia, the successful first computations of the Dynamical Cooperative Decay Rate and the Dynamical Cooperative Lamb Shift [1], the time-varying angular distribution profile of emitted radiation in the superradiance emission from a sphere [2], and most recently the establishment of relations among the frequency and the pumping threshold of cw lasing from an open (no end-mirrors) system with the dominant eigenmode eigenvalue [3]. The eigenmodes and their spectral analysis for both the one-dimensional (1D) (slab) geometry [4,5] and the spherical geometry [6–8] have already been obtained; however, these geometries do not describe the important cases of fibers, nanotubes, and nanowires. Obtaining the spectral analysis expansions for the infinite cylindrical geometry are necessary for analyzing the collective dynamics of an ensemble of atoms in this shape. The group of Stone at Yale has previously given the expressions for the eigenfunctions and the eigenvalues for the infinite cylinder [9]. I shall quickly review their results here for completeness sake, and as a prelude to obtaining the expressions of the Fourier-like expansion for an arbitrary prepared initial state of the system. This allows one to directly obtain the temporal development of the state of the system in the linear regime of superradiance. (The same technique can as well be used if one is considering the decay from a system when only few atoms have been excited—the time development in this case is directly obtained by changing the sign of any mode eigenvalues in the Fourier-like expansion of the state of the system.)

In Sec. II, I review the details of how to obtain the eigenmodes for the kernel in this geometry, using the same steps that R. Friedberg and I used for the sphere and the slab (3), (4), and (6). Both the expressions of the complex wave vectors and eigenvalues for this symmetric but non-Hermitian operator are obtained replicating the results of [9]. In Sec. III, I find the proper metric for the scalar product of two eigenmodes modes and the normalization constant for any eigenmode. A Fourier-like expansion of an initial state of the system becomes then possible. In Sec. IV, I obtain the time development of an initially uniformly prepared inverted system. I show that a temporal modulation develops in the atomic excitation state function for a cylinder satisfying the condition ($r = m\lambda, m$ integer) (i.e., when the system has two co-dominant modes). In Sec. V, I show that the same cylindrical system but now initially prepared in a phased state will develop what appears as a chaotic angular distribution. I show that this is the result of the high multiplicity of modes having close values of the real part of their eigenvalue.

II. DETERMINING THE EIGENMODES

A. Integral equation of the state function of the atomic excitation

The state function of the atomic excitation in the scalar photon theory, $b(\vec{r},t)$, obeys the integral equation [6,7]:

$$\dot{b}(\vec{r},t) = -\frac{\gamma_1}{2} b(\vec{r},t) - \frac{\mu^2}{\hbar}\frac{N}{V}\int d^3\vec{r}\,' \frac{\exp(ik_0|\vec{r}-\vec{r}\,'|)}{i|\vec{r}-\vec{r}\,'|} b(\vec{r}\,',t), \tag{2.1}$$

where γ_1, the isolated atom decay rate, is given by

$$\gamma_1 = \frac{2\mu^2}{\hbar c}\omega_0, \tag{2.2}$$

and where N is the total number of two-level atoms. The kernel of this integral equation is the simplified form of the Lienard-Wiechert potential [10].

For the steady state, Eq. (2.1) can be written inside the medium as

$$\left(i\omega - i\omega_0 - \frac{\gamma_1}{2}\right) b(\vec{r}) = \frac{\mu^2}{\hbar}\frac{N}{V}\int d^3\vec{r}\,' \frac{\exp(ik_0|\vec{r}-\vec{r}\,'|)}{i|\vec{r}-\vec{r}\,'|} b(\vec{r}\,'). \tag{2.3}$$

*jmanassah@gmail.com

We are using here the interaction picture of quantum mechanics.

B. Differential form

Following closely the derivation in [6] for the spherical geometry, defining a classical field $\Phi(\vec{r})$ by

$$\Phi(\vec{r}) = \int d^3\vec{r}'\rho(\vec{r}')\frac{\exp(ik_0|\vec{r}-\vec{r}'|)}{|\vec{r}-\vec{r}'|}b(\vec{r}'), \tag{2.4}$$

where $\rho(\vec{r})$ is the local number density, and using the familiar form of the Green's function for the Helmholtz equation,

$$\left(\nabla^2 + k_0^2\right)\frac{\exp(ik_0|\vec{r}-\vec{r}'|)}{|\vec{r}-\vec{r}'|} = -4\pi\delta^3(\vec{r}-\vec{r}'), \tag{2.5}$$

one obtains

$$\left(\nabla^2 + k_0^2\right)\Phi(\vec{r}) = -4\pi b(\vec{r})\rho(\vec{r}). \tag{2.6}$$

Now, multiplying (2.3) on both sides by $4\pi\rho(\vec{r})$, one obtains inside the medium,

$$\left(\nabla^2 + k_0^2 - \frac{4\pi\mu^2}{\hbar c}\frac{N}{V}\frac{1}{k-k_0+i\gamma_1/2c}\right)\Phi(\vec{r}) = 0, \tag{2.7}$$

while outside the medium, the classical "field" $\Phi(\vec{r})$ obeys the differential equation,

$$\left(\nabla^2 + k_0^2\right)\Phi(\vec{r}) = 0 \tag{2.8}$$

C. Determining the wave vector inside the medium

The wave vector inside the medium is directly determined from the conditions that both the "field" and its derivative are continuous at the boundary separating the two-level medium from vacuum.

For the two-dimensional problem (i.e., no z dependence), inside the cylinder ($r < a$) (2.7) reduces to

$$\left(\nabla_T^2 + k'^2\right)\Phi(\vec{r}) = 0, \tag{2.9}$$

where k' is given by

$$k'^2 = k_0^2 - \frac{4\pi\mu^2}{\hbar c}\frac{N}{V}\frac{1}{k-k_0+i\gamma_1/2c}, \tag{2.10}$$

while outside the cylinder ($r > a$), (2.8) reduces to

$$\left(\nabla_T^2 + k_0^2\right)\Phi(\vec{r}) = 0. \tag{2.11}$$

The valid solutions of (2.9) are those regular at the origin, and for (2.11) those outgoing at infinity. The boundary conditions are

$$\Phi(r = a^-) = \Phi(r = a^+), \tag{2.12}$$

$$\left.\frac{d\Phi}{dr}\right|_{r=a^-} = \left.\frac{d\Phi}{dr}\right|_{r=a^+}. \tag{2.13}$$

Looking for separable solutions of the differential equation of the form,

$$\Phi(r,\varphi) = R(r)\exp(im\varphi), \tag{2.14}$$

the ordinary differential equation (ODE) for $R(r)$ inside the cylinder is

$$\frac{d^2R}{dr^2} + \frac{1}{r}\frac{dR}{dr} - \frac{m^2}{r^2}R + k'^2R = 0, \tag{2.15}$$

while outside the cylinder it is given by

$$\frac{d^2R}{dr^2} + \frac{1}{r}\frac{dR}{dr} - \frac{m^2}{r^2}R + k_0^2R = 0. \tag{2.16}$$

Introducing the normalized coordinates,

$$v = k'a \quad u_0 = k_0a \quad x = r/a,$$

the solutions of the ODE satisfying the conditions of regularity at the origin for (2.15), and the outgoing wave solution for (2.16) at infinity are, respectively,

$$R(x) = \begin{cases} C_1J_m(vx) & x < 1 \\ C_2H_m^{(1)}(u_0x) & x > 1. \end{cases} \tag{2.17}$$

The boundary conditions (2.12) and (2.13) and the solutions (2.17) uniquely determine the transcendental equation that should be satisfied by v, the complex wave vector, namely the condition already obtained in [9]

$$\frac{vJ_m'(v)}{J_m(v)} = \frac{u_0H_m^{(1)'}(u_0)}{H_m^{(1)}(u_0).} \tag{2.18}$$

This expression can be simplified by using the standard recursion relations for the Bessel function $Z_m(x)$,

$$\frac{dZ_m(x)}{dx} = \frac{1}{2}[Z_{m-1}(x) - Z_{m+1}(x)], \tag{2.19}$$

and

$$Z_{m-1}(x) + Z_{m+1}(x) = \frac{2m}{x}Z_m(x). \tag{2.20}$$

From (2.19) and (2.20) one obtains

$$vZ_m'(v) = vZ_{m-1}(v) - mZ_m(v), \tag{2.21}$$

which combined with (2.18) give the transcendental equation that more easily determines v in numerical calculations,

$$\frac{vJ_{m-1}(v)}{J_m(v)} = \frac{u_0H_{m-1}^{(1)}(u_0)}{H_m^{(1)}(u_0)}. \tag{2.22}$$

Note that for each value of m, this equation admits an infinite number of solutions which can be indexed by the radial subscript s. Henceforth, I shall subscript the v's by two indices $\{m,s\}$ and refer to these, respectively, as the azimuthal and radial indices.

I plot in Figs. 1(a) and 1(b) the real and imaginary parts of this complex wave vector as a function of u_0 for the three lowest indices for $u_0 < 2\pi$.

I plot in Figs. 2(a) and 2(b) the imaginary part of v as a function of the real part of v for selected values of m, for the different values of the radial index, and for the cylinder having $u_0 = 12\pi$ (i.e., $a = 6\lambda$).

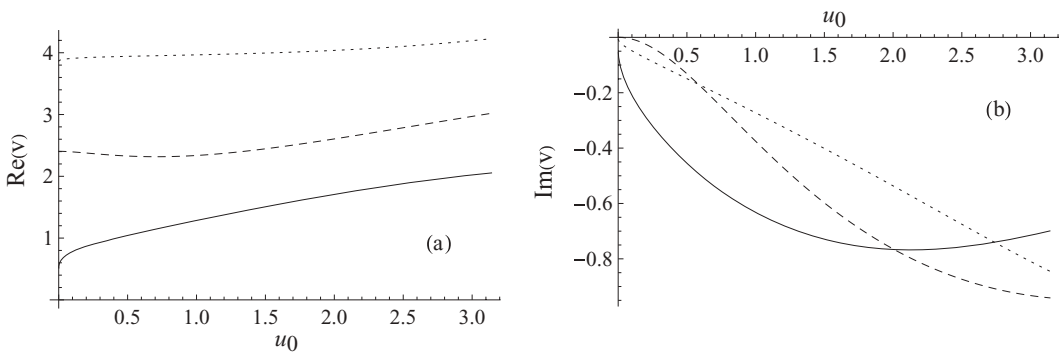

FIG. 1. The real (a) and the imaginary (b) parts of the wave vectors for the lowest order modes are plotted as a function of u_0. (Solid line) $m = 0, s = 1$; (dashed line) $m = 1, s = 1$; (dotted line) $m = 0, s = 2$.

D. Eigenvalues

The eigenvalues can be directly obtained from (2.10). Specifically,

$$\lambda = \frac{4\pi\mu^2}{\hbar c}\frac{Na^2}{V}\frac{i}{u_0^2 - v^2} = \frac{2\gamma_1 c}{\omega_0}\sigma\frac{i}{u_0^2 - v^2}, \qquad (2.23)$$

where $\sigma = N/L$. Defining $C' = \frac{2\gamma_1 c\sigma}{\omega_0}$, the normalized eigenvalues are

$$\Lambda_{m,s} = \frac{\lambda_{m,s}}{C'} = \frac{i}{u_0^2 - v_{m,s}^2}. \qquad (2.24)$$

It is to be noted that, as defined in (2.24), $\mathrm{Re}(\Lambda_{m,s})$ determines the rate of growth (decay, if the sign is changed) of the mode $\{m,s\}$, while $\mathrm{Im}(\Lambda_{m,s})$ determines its shift.

In Fig. 3, I plot the real part of the normalized eigenvalues for the lowest order indices as function of u_0 for $u_0 < 2\pi$. Note that $\mathrm{Re}(\Lambda_{0,1})$ is much larger than the corresponding quantity for the other modes for $u_0 \ll 1$, and thus the mode $\{m = 0, s = 1\}$ dominates the superradiance dynamics at large time for this range of values of u_0. Hence one can infer that for this range of u_0, irrespective of the initial state, the dynamics of the system is uniquely determined by the $\{m = 0, s = 1\}$ eigenmode.

I plot in Figs. 4 and 5 the real and imaginary parts of the normalized eigenvalues for, respectively, $u_0 = 12\pi$ and $u_0 = 12.25\pi$, as function of the radial index for the azimuthal number $m = 0$. Note that for $u_0 = 12\pi$, the modes with $s = 12$ and $s = 13$ have almost equal values for the real part of their eigenvalues. This will prove essential for understanding the time development of superradiance for samples with $u_0 = p\pi$, where p is an integer, which have been initially prepared in a uniform and isotropical initial state.

III. PROPERTIES OF THE EIGENFUNCTIONS

A. Orthogonality of the eigenfunctions

Given that the kernel of the integral equation is not Hermitian but symmetric, the orthogonality relationship, as usually defined by the standard scalar product in Hilbert space between any two eigenfunctions with the same azimuthal index but different radial indices, will not be satisfied here. Instead, the following "orthogonality" relation is satisfied:

$$\int_0^1 dx\, x J_m\left(v_{m,s_1}x\right) J_m\left(v_{m,s_2}x\right) = 0, \qquad (3.1)$$

where $s_1 \neq s_2$.

Proof. Since this "orthogonality" condition can be derived in few steps, I shall do so without invoking any of the general properties of symmetric operators. It should be remembered that in going from discrete to infinite dimensions, the metric in the scalar product is not always trivially apparent. See, for example, how the scalar product had to be defined for the electric eigenmodes of a sphere [8] so that its definition is consistent with the boundary conditions of the problem.

From the standard integral for Bessel functions,

$$\int_0^1 dx\, x J_m\left(v_{m,s_1}x\right) J_m\left(v_{m,s_2}x\right) = \frac{\left[v_{m,s_2} J_{m-1}\left(v_{m,s_2}\right) J_m\left(v_{m,s_1}\right) - v_{m,s_1} J_{m-1}\left(v_{m,s_1}\right) J_m\left(v_{m,s_2}\right)\right]}{v_{m,s_1}^2 - v_{m,s_2}^2}, \qquad (3.2)$$

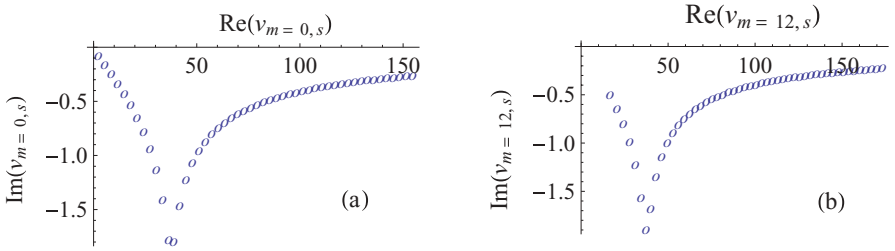

FIG. 2. (Color online) (a) $\mathrm{Im}(v_{0,s})$ is plotted as a function of $\mathrm{Re}(v_{0,s})$; (b) $\mathrm{Im}(v_{12,s})$ is plotted as function of $\mathrm{Re}(v_{12,s})$. $u_0 = 12\pi$.

combined with (2.22) and the right-hand side of (3.2), one obtains

$$\int_0^1 dx\, x J_m\left(v_{m,s_1}x\right) J_m\left(v_{m,s_2}x\right) = \frac{\left[J_m\left(v_{m,s_2}\right)\frac{u_0 H_{m-1}(u_0)}{H_m(u_0)} J_m\left(v_{m,s_1}\right) - J_m\left(v_{m,s_1}\right)\frac{u_0 H_{m-1}(u_0)}{H_m(u_0)} J_m\left(v_{m,s_2}\right)\right]}{v_{m,s_1}^2 - v_{m,s_2}^2} = 0, \tag{3.3}$$

which is the desired result.

B. Normalization of the eigenfunctions

The normalization of the eigenfunctions are directly obtained from the standard Bessel functions integral,

$$\int_0^1 dx\, x J_m\left(v_{m,s_1}x\right) J_m\left(v_{m,s_1}x\right) = \frac{1}{2}\left(J_m^2\left(v_{m,s_1}\right) - \frac{2m J_m\left(v_{m,s_1}\right) J_{m+1}\left(v_{m,s_1}\right)}{v_{m,s_1}} + J_{m+1}^2\left(v_{m,s_1}\right)\right). \tag{3.4}$$

For the special case, $m = 0$,

$$\int_0^1 dx\, x J_0\left(v_{0,s_1}x\right) J_0\left(v_{0,s_1}x\right) = \frac{1}{2}\left[J_0^2\left(v_{0,s_1}\right) + J_1^2\left(v_{0,s_1}\right)\right]. \tag{3.5}$$

C. Eigenfunction expansion of unity

Using (3.3), (3.5), and the closed-form integral,

$$\int_0^1 dx\, x J_0(v_{0,s}x) = \frac{J_1(v_{0,s})}{v_{0,s}}, \tag{3.6}$$

an arbitrary constant can be directly expanded in the eigenfunctions having zero azimuthal index to obtain

$$1 = \sum_s \frac{J_1(v_{0,s})}{v_{0,s}\left\{\frac{1}{2}\left[J_0^2(v_{0,s}) + J_1^2(v_{0,s})\right]\right\}} J_0(v_{0,s}x). \tag{3.7}$$

It is to be noted that everywhere in the interval $0 < x < 1$ the deviation between the numerical value of the reconstituted function [right-hand side of (3.7)] and the function $y = 1$ is less than one per thousand if one includes in the (3.7) sum the lowest 200 eigenfunctions with azimuthal index ($m = 0$). I have maintained this level of accuracy throughout.

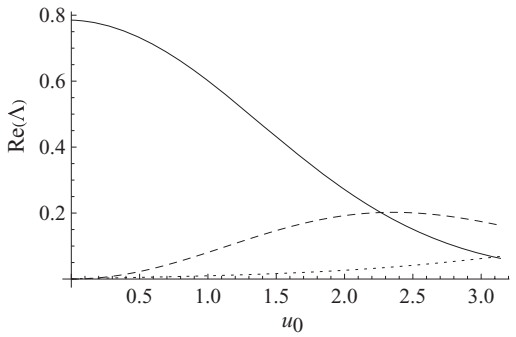

FIG. 3. $\mathrm{Re}(\Lambda_{m,s})$ is plotted as a function of u_0 for the lowest order modes. (Solid line) $m = 0, s = 1$; (dashed line) $m = 1, s = 1$; (dotted line) $m = 0, s = 2$.

IV. DYNAMICS OF SUPERRADIANCE FOR A SYSTEM THAT IS INITIALLY UNIFORMLY AND ISOTROPICALLY PREPARED

The time development of $b(\vec{r},t)$ for an initially completely inverted system with the initial condition $b(\vec{r},0) = 1$ can be directly obtained from (3.7) and (2.24), specifically,

$$b(x = r/a, T) = \sum_s \frac{J_1(v_{0,s})}{v_{0,s}\left\{\frac{1}{2}\left[J_0^2(v_{0,s}) + J_1^2(v_{0,s})\right]\right\}} J_0(v_{0,s}x)\exp(\Lambda_{0,s}T), \tag{4.1}$$

where $T = C't$.

In Fig. 6, I plot $b\,(x = 1, T)$ as a function of the normalized time T for, respectively, $u_0 = 12\pi$ and $u_0 = 12.25\pi$.

For $u_0 = 12.25\pi$, there is only one dominant mode [i.e., the mode with the largest value of $\mathrm{Re}(\Lambda_{0,s})$] as can be verified by examining Fig. 5(a). This mode completely describes the dynamics of superadiance for large T. The slope of the natural logarithmic graph is equal to $\mathrm{Re}(\Lambda_{0,13}) = 0.006\,337$.

On the other hand, for $u_0 = 12\pi$, two modes have almost equal values of $\mathrm{Re}(\Lambda)$, specifically,

$$\mathrm{Re}(\Lambda_{0,12}) = 0.004\,9527 \quad \text{and} \quad \mathrm{Re}(\Lambda_{0,13}) = 0.004\,9717.$$

In the domain of interest (i.e., late linear regime of superradiance), these co-dominant modes coherently add up and the magnitude of their resultant depends on the relative phase between the two modes. The separation between two consecutive minima of $|b(x,T)|$ is given by

$$\Delta T = \frac{2\pi}{|\mathrm{Im}(\Lambda_{0,12}) - \mathrm{Im}(\Lambda_{0,13})|}. \tag{4.2}$$

Substituting the values,

$$\mathrm{Im}(\Lambda_{0,12}) = 0.003\,7396 \quad \text{and} \quad \mathrm{Im}(\Lambda_{0,13}) = -0.003\,3353,$$

in (4.2), one obtains $\Delta T \cong 888$, which is the value obtained in the computation of Fig. 7(a).

It is important to note that although the temporal modulational frequency is the same for all values of x, the positions of these temporal minima is different for different values of x. This is caused by the x-dependent extra phase shift contributed by the terms $J_0(v_{0,12}x)$ and $J_0(v_{0,13}x)$ multiplying, respectively, $\exp(\Lambda_{0,12}T)$ and $\exp(\Lambda_{0,13}T)$ in (4.1). The different spatial dependence in the value of $|b|$ can for large T be directly deduced by following the spatial dependence of the real and imaginary parts of the contribution of each of the dominant modes to the total state function. I plot in Figs. 7 and 8 the spatial distribution of the real and imaginary parts of the contributions of each of the dominant modes to b, and the value of $|b|$ for two values of T. In Fig. 7, $|b|$ is maximum at $x = 0$; and in Fig. 8, $|b|$ is maximum at $x = 1$.

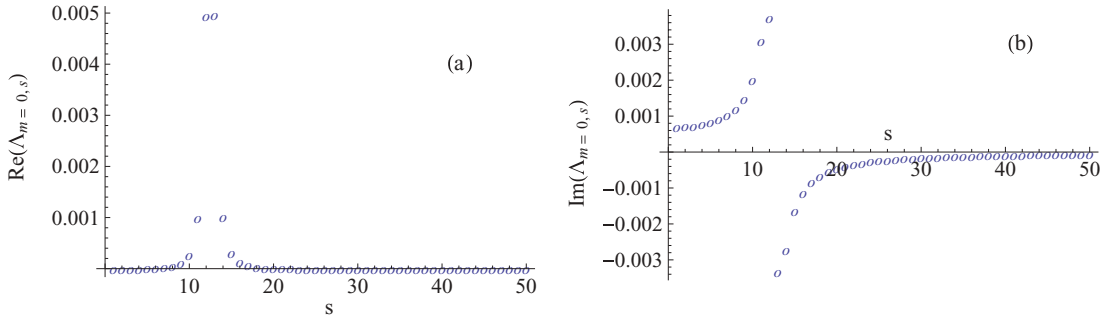

FIG. 4. (Color online) (a) $\mathrm{Re}(\Lambda_{0,s})$ and (b) $\mathrm{Im}(\Lambda_{0,s})$ are plotted as functions of the radial index. $u_0 = 12\pi$.

The spatial distribution of $|b|$ [Figs. 7(c) and 8(c)] can be read off directly, respectively, from Figs. 7(a) and 7(b), and from Figs. 8(a) and 8(b), and recalling that both dominant eigenfunctions are zero-order Bessel functions with arguments differing approximately at $x = 1$ by π.

V. DYNAMICS OF SUPERRADIANCE FOR A SYSTEM INITIALLY PREPARED IN A PHASED STATE.

I shall first remind the reader of the expression giving the expansion of an exponential function in an infinite series of Bessel functions. This expression shall prove useful in computing the expansion coefficients of an initially prepared phased state.

Recalling that the generating function of the Bessel functions is given by

$$\exp\left[\frac{\zeta}{2}\left(t-\frac{1}{t}\right)\right] = \sum_{n=-\infty}^{\infty} J_n(\zeta)t^n, \tag{5.1}$$

if one sets $t = i\exp(i\varphi)$, then

$$\frac{\zeta}{2}\left(t-\frac{1}{t}\right) = i\frac{\zeta}{2}[\exp(i\varphi)+\exp(-i\varphi)] = i\zeta\cos(\varphi), \tag{5.2}$$

and (5.1) can be rewritten as

$$\exp[i\zeta\cos(\varphi)] = \sum_{n=-\infty}^{\infty} J_n(\zeta)i^n\exp(in\varphi). \tag{5.3}$$

Equation (5.3) can be further simplified if one notes that the left-hand side of (5.1) is invariant under the substitution $t \to -\frac{1}{t}$. Comparing the right-hand side of the original and transformed expressions, one obtains

$$i^n J_n(\zeta) = i^{-n} J_{-n}(\zeta). \tag{5.4}$$

Combining (5.3) with (5.4), one obtains

$$\exp[i\zeta\cos(\varphi)] = J_0(\zeta) + 2\sum_{n=1}^{\infty} J_n(\zeta)i^n\cos(n\varphi). \tag{5.5}$$

Using this expansion, it is then straightforward to find the Fourier-like expansion of the initial phased state $b(\vec{r},t=0) = \exp[iu_0x\cos(\varphi)]$ in the previously defined eigenfunctions basis.

If we write

$$b_{\mathrm{ph}}(\vec{r},t=0) = \sum_{m=0}^{\infty}\sum_{s=1}^{\infty} A(m,s)J_m(v_{m,s}x)\cos(m\varphi), \tag{5.6}$$

where the subscript ph is to remind the reader that this quantity refers to the phased initial state function. Combining (3.2) and (5.5), we deduce

$$\begin{aligned} A(0,s) &= \frac{\int_0^1 dx\,x J_0(u_0x)J_0(v_{0,s}x)}{\int_0^1 dx\,x J_0(v_{0,s}x)J_0(v_{0,s}x)} \\ &= \frac{2[u_0J_0(v_{0,s})J_1(u_0) - v_{0,s}J_0(u_0)J_1(v_{0,s})]}{\left(u_0^2 - v_{0,s}^2\right)\left(J_0^2(v_{0,s}) + J_1^2(v_{0,s})\right)}, \end{aligned} \tag{5.7}$$

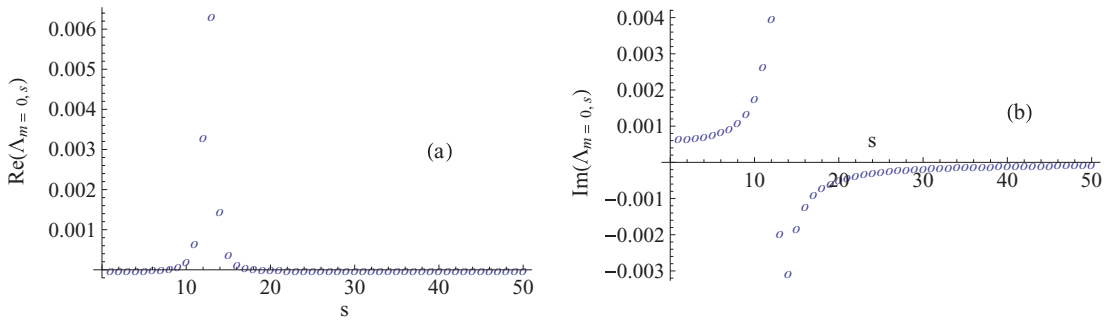

FIG. 5. (Color online) (a) $\mathrm{Re}(\Lambda_{0,s})$ and (b) $\mathrm{Im}(\Lambda_{0,s})$ are plotted as functions of the radial index. $u_0 = 12.25\pi$.

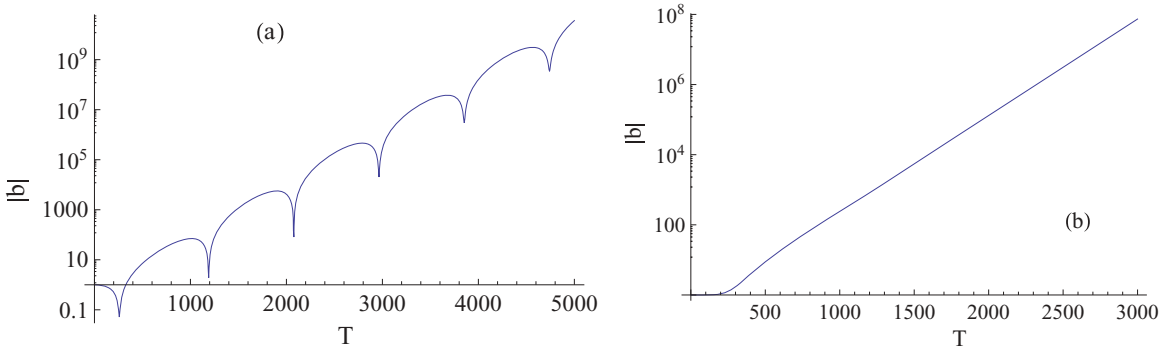

FIG. 6. (Color online) For the initially inverted uniform state, the magnitude of the atomic excitation state function is plotted as a function of the normalized time at $r/a = x = 1$. (a) $u_0 = 12\pi$. (b) $u_0 = 12.25\pi$.

for $m = 0$, and

$$A(m,s) = 2i^m \frac{\int_0^1 dx x J_m(u_0 x) J_m(v_{m,s} x)}{\int_0^1 dx x J_m(v_{m,s} x) J_m(v_{m,s} x)} = 4i^m \frac{[v_{m,s} J_{m-1}(v_{m,s}) J_m(u_0) - u_0 J_{m-1}(u_0) J_m(v_{m,s})]}{(u_0^2 - v_{m,s}^2)\left[J_{m-1}^2(v_{m,s}) - \left(\frac{2m}{v_{m,s}}\right) J_{m-1}(v_{m,s}) J_m(v_{m,s}) + J_m^2(v_{m,s})\right]}, \tag{5.8}$$

for $m \neq 0$.

The expression for $b(\vec{r},T)$ is then given by

$$b_{\rm ph}(\vec{r},T) = \sum_{m=0}^{\infty} \sum_{s=1}^{\infty} A(m,s) J_m(v_{m,s} x) \cos(m\varphi) \exp(\Lambda_{m,s} T). \tag{5.9}$$

(The figures shown in this section are obtained by numerically summing this double series; 9600 modes are included in these sums.)

I plot in Figs. 9 and 10, $|b_{\rm ph}(x,T)|$ as function of the azimuthal angle for, respectively, the normalized radial distances $x = 1$ and $x = 1/2$ at different values of T.

One notes the following:

(i) The change in scale between the values of $|b(x,T)|$ in Fig. 8 and those in Figs. 9 and 10 is due to the fact that $\max[\mathrm{Re}(\Lambda_{0,s})] = 0.004\,9717$, while $\max[\mathrm{Re}(\Lambda_{m,s})] = 0.007\,1519$.

(ii) The apparent chaotic behavior in the positions of the maxima in Figs. 9 and 10 is simply a manifestation of the large number of modes with real values close to that of the dominant mode, namely if one orders the different eigenmodes as per the decreasing value of the real part of their eigenvalues, one

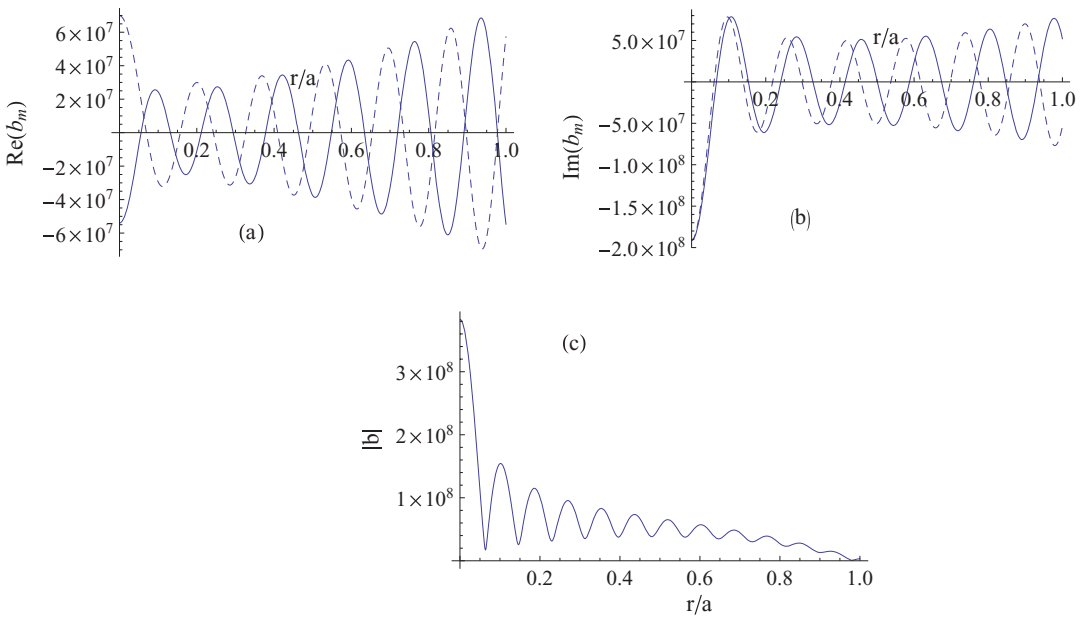

FIG. 7. (Color online) (a) The real part and (b) the imaginary part of the contributions from the $s = 12$ (solid line) and the $s = 13$ (dashed line) modes, and (c) the magnitude of the sum from all modes to the atomic excitation state function are plotted as functions of the normalized radius, for an initially inverted uniform state. $T = 3852$. $u_0 = 12\pi$.

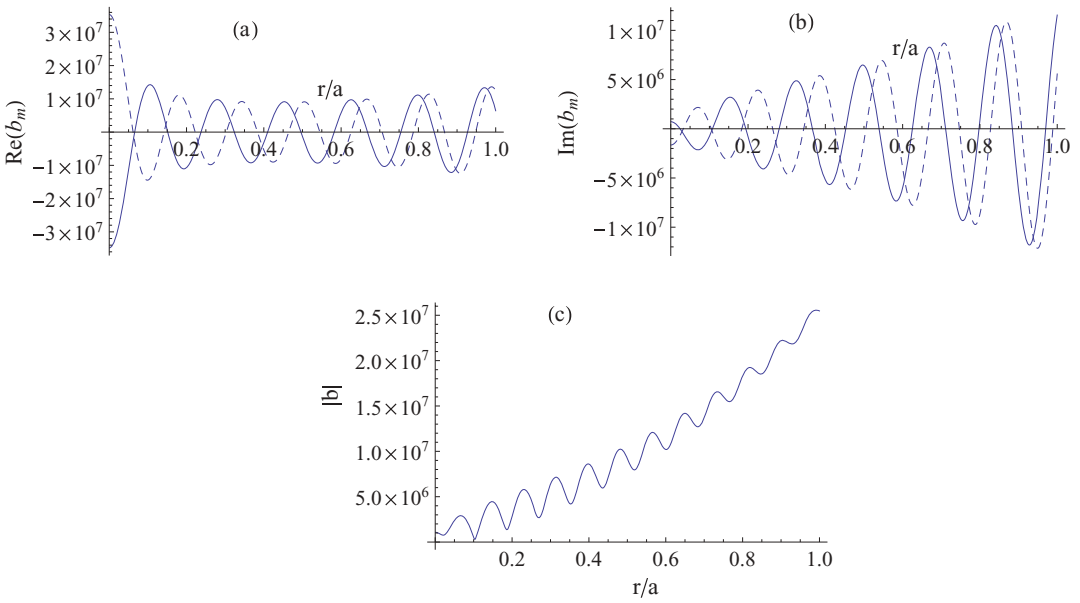

FIG. 8. (Color online) (a) The real part and (b) the imaginary part of the contributions from the $s = 12$ (solid line) and the $s = 13$ (dashed line) modes, and (c) the magnitude of the sum from all modes to the atomic excitation state function are plotted as functions of the normalized radius, for an initially inverted uniform state. $T = 3500$. $u_0 = 12\pi$.

obtains the following:

$$\text{Ordered}\{\text{Re}(\lambda_{m,s})\} = \{0.007\,1519, 0.007\,1278, 0.007\,0022, 0.006\,9962, 0.006\,9261, 0.006\,8693, 0.006\,7135, 0.006\,6359, 0.006\,6328, 0.006\,5800, 0.006\,5283, \ldots.\}.$$

It is to be noted that the previously mentioned modes do not all have the same values for their azimuthal number, thus the nonsimilarity of the angular distribution at different values of the radius. The corresponding values of $\exp[\text{Re}(\Lambda_{m,s})(T = 3500)]$ for the previous array are

$$\{7.43166 \times 10^{10}, 6.83072 \times 10^{10}, 4.40077 \times 10^{10}, 4.31027 \times 10^{10}, 3.37152 \times 10^{10}, 2.76448 \times 10^{10}, 60231 \times 10^{10}, 1.22076 \times 10^{10}, 1.20799 \times 10^{10}, 1.00422 \times 10^{10}, 8.37864 \times 10^{9}\},$$

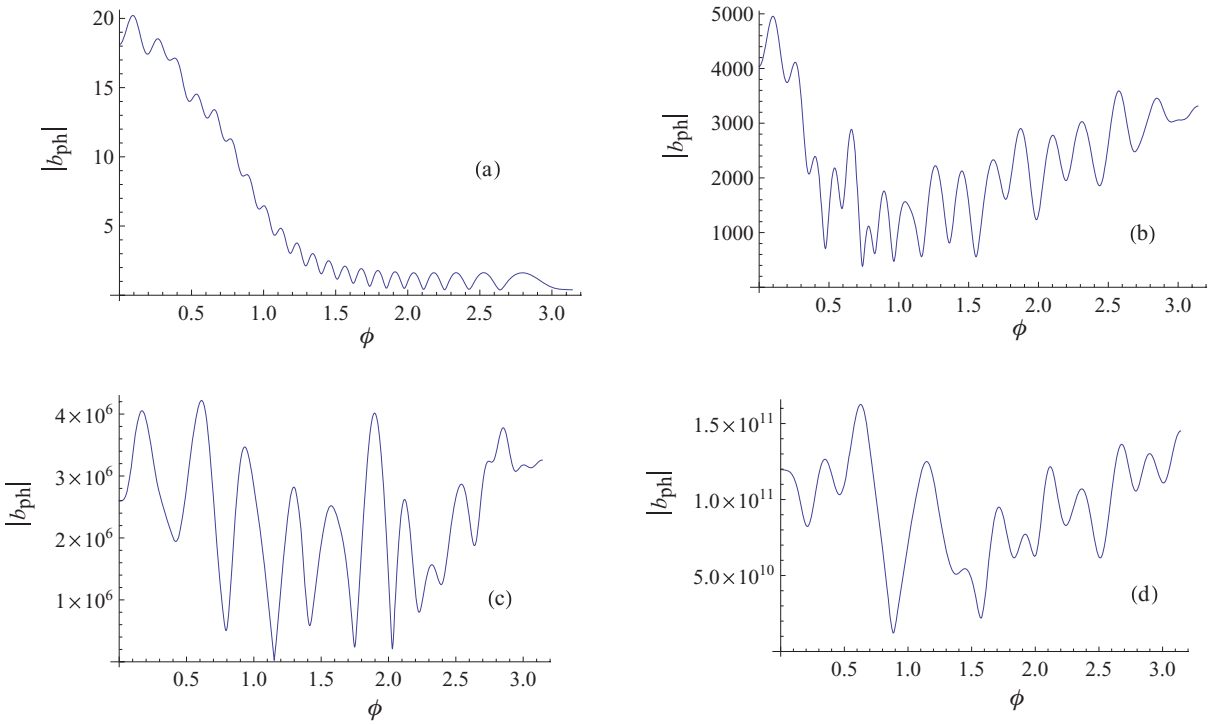

FIG. 9. (Color online) For the initially inverted phased state, the magnitude of the atomic excitation state function is plotted as a function of the azimuthal angle, for the normalized radial distance $x = 1$. (a) $T = 200$. (b) $T = 1000$. (c) $T = 2000$. (d) $T = 3500$. $u_0 = 12\pi$.

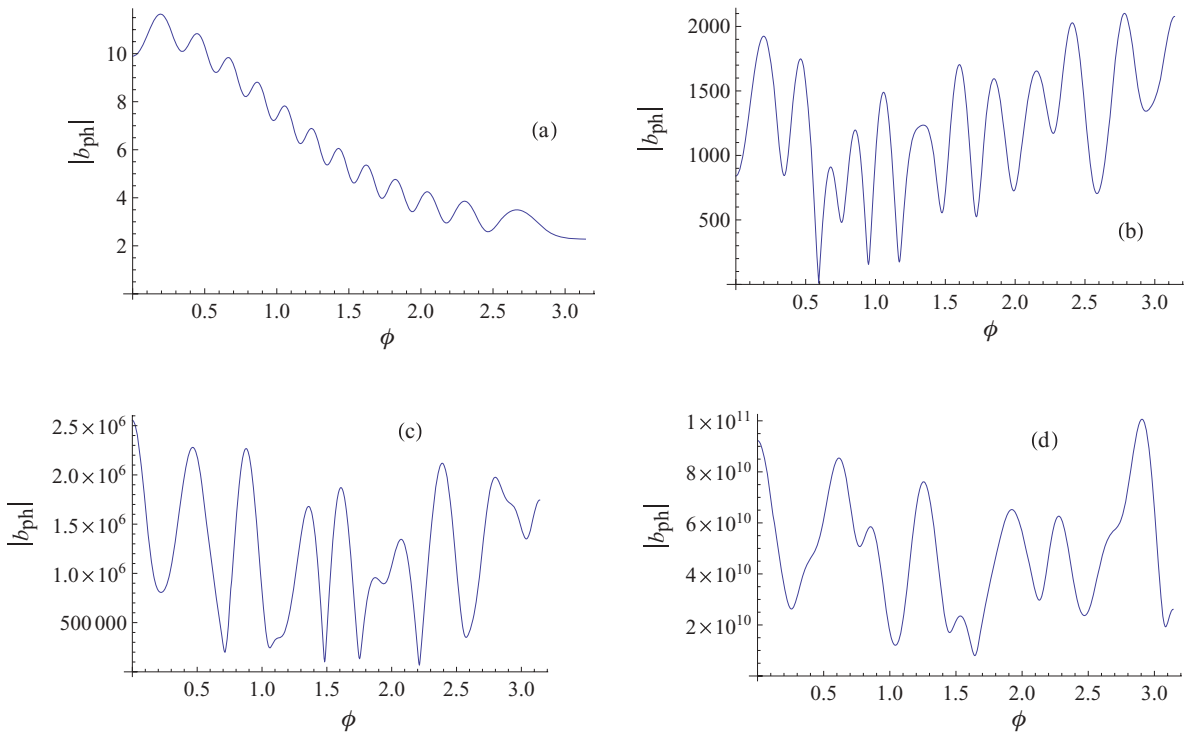

FIG. 10. (Color online) For the initially inverted phased state, the magnitude of the atomic excitation state function is plotted as a function of the azimuthal angle, for the normalized radial distance $x = 1/2$. (a) $T = 200$. (b) $T = 1000$. (c) $T = 2000$. (d) $T = 3500$. $u_0 = 12\pi$.

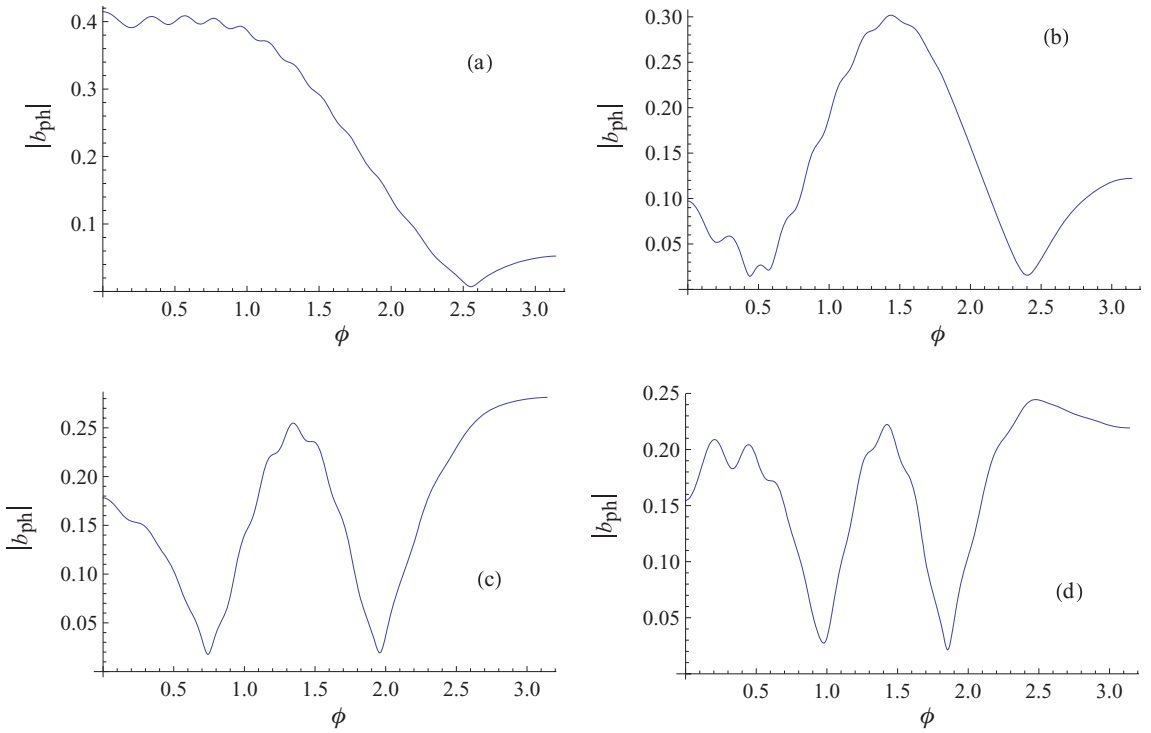

FIG. 11. (Color online) For a system initially with few excited atoms prepared in the phased state, the magnitude of the atomic excitation state function is plotted as a function of the azimuthal angle, for the normalized radial distance $x = 1/2$. (a) $T = 200$. (b) $T = 1000$. (c) $T = 2000$. (d) $T = 3500$. $u_0 = 12\pi$.

that is, the leading 11 modes each contribute to the state function a value exceeding 10% of the contribution of the dominant mode in the (5.9) sum.

(iii) The irregularity in the angular distribution found for the case of superradiance from an inverted system appears, at first sight, present in the emission distribution from a system with only few atoms initially excited by a weak stream of photons impinging on the cylinder in a direction perpendicular to the cylinder axis, and having their polarization parallel to the cylinder's axis. I show in Fig. 11, the angular distribution of the state function at a radial distance equal to half the radius of the cylinder for different values of T. However, using the Eikonal-SVEAS (Slowly-Varying-Envelope-Approximation-in-Space) approximation developed in [11], one can predict the main features appearing in Fig. 11 rather well. I shall discuss elsewhere the reasons for the validity of this approximation in the case of the low excitation case, but not for the fully inverted atoms case.

In conclusion, the state function spatial dependence at different times for a system of a cloud of two-level atoms spatially uniformly dispersed over an infinite cylindrical shape with radius larger than a few wavelengths of the transition radiation, that was initially inverted exhibits complex features which are not, a priori, obvious. A full spectral analysis of the problem is required for a proper understanding of the problem's features.

ACKNOWLEDGMENTS

It is my pleasure to acknowledge valuable discussions with Richard Friedberg.

[1] R. Friedberg and J. T. Manassah, Phys. Lett. A **373**, 3423 (2009); J. T. Manassah, Laser Phys. **20**, 259 (2010).
[2] R. Friedberg and J. T. Manassah, Opt. Commun. **281**, 4391 (2008); **282**, 3089 (2009).
[3] R. Friedberg and J. T. Manassah, Phys. Lett. A **374**, 3389 (2010).
[4] R. Friedberg and J. T. Manassah, Phys. Lett. A **372**, 2787 (2008).
[5] S. Prasad and R. J. Glauber, Phys. Rev. A **61**, 063814 (2000).
[6] R. Friedberg and J. T. Manassah, Phys. Lett. A **372**, 2541 (2008).
[7] A. A. Svidzinsky, J. T. Chang, and M. O. Scully, Phys. Rev. A **81**, 053821 (2010).
[8] R. Friedberg and J. T. Manassah, Phys. Lett. A **373**, 4416 (2009).
[9] H. E. Tureci, A. Douglas Stone, and B. Collier, Phys. Rev. A **74**, 043822 (2006).
[10] M. J. Stephen, J. Chem. Phys. **40**, 669 (1964).
[11] R. Friedberg and J. T. Manassah, Laser Phys. **20**, 250 (2010).